

Enhanced Physical and Mechanical Properties of Flake–Shape/Vinyl-ester Nanocomposites Through Surface Modification of Graphene and Glass Flake: A Comparison with Simulated Data

Hamed Mohammad Gholiha¹, Azam Ghadami^{2,*} , Majid Monajjemi² , Morteza Ehsani^{3,4,*} 

¹ Department of Polymer Engineering, Science and Research Branch, Islamic Azad University, Tehran, Iran

² Department of Chemical Engineering, Faculty of Engineering, Central Tehran Branch, Islamic Azad University, Tehran, Iran

³ Plastic Department, Iran Polymer and Petrochemical Institute (IPPI), Tehran, Iran

⁴ Department of Polymer Engineering, Faculty of Engineering, South Tehran Branch, Islamic Azad University, Tehran, Iran

* Corresponding author: M.ehsani@ippi.ac.ir (M.E.); A.ghadami1394@gmail.com, A.ghadami@iauctb.ac.ir (A.G.);

Scopus Author ID 6701810683

Received: 3.11.2020; Revised: 30.11.2020; Accepted: 2.12.2020; Published: 10.12.2020

Abstract: The main goal of this work was to investigate the effects of silane-modified graphene nanosheets (MGNS) and modified nanoglass flakes (MNGF) on the physical and mechanical properties of vinyl-ester resin (VER) composites. The surface modification was evaluated about these composites' physical and mechanical behavior by techniques such as water absorption, tensile, three-point bending, and dynamic mechanical thermal analysis (DMTA). The analytical data revealed that the silane functionalized nanocomposites improved the interface between the nanosheets and vinyl-ester matrix. It was found that surface modification could significantly improve the dispersion and adhesion of GNS and nanoglass flakes (NGF) compared with those of neat vinyl-ester and unmodified composites. The presence functionalization of NGF and graphene nanosheets (GNS) in vinyl-ester formulation did affect the tensile and flexural strength and modulus, water absorption, and storage modulus. GNS/VER exhibited higher tensile and flexural strength and modulus than the original composite. DMTA results also showed incorporation of NGF and GNS decreased glass transition and increased storage modulus relative to neat composites. Nonetheless, the incorporation of functionalized graphene nanosheets and nano glass flakes represent higher Tg and storage modulus.

Keywords: graphene surface modification; glass flake surface modification; vinyl-ester nanocomposite; physical and mechanical properties.

© 2020 by the authors. This article is an open-access article distributed under the terms and conditions of the Creative Commons Attribution (CC BY) license (<https://creativecommons.org/licenses/by/4.0/>).

1. Introduction

Vinyl-ester resins are thermoset polymers obtained by an addition reaction between epoxy resin (difunctional or multifunctional) with unsaturated carboxylic acid monomers methacrylic acid. The unique physical and chemical properties of vinyl-ester resins (VE) have attracted much interest for marine industrial applications. VE resin exhibits desirable mechanical properties like epoxy and simultaneously offers processability like a polyester resin. VERs are the most important thermosets that are widely used in industrial goods. For example, VER can substitute polyester resin for marine coatings and adhesives application to enhance or provide physical properties. The vinyl-ester resin can be reinforced with different types of fillers and fibers such as carbon black, clay, carbon, and glass fibers, incorporated in

these resins that caused to improve modulus, thermal expansion, thermal, and electrical conductivity.[1-3]. Nonetheless, commonly nanofiller reinforced polymeric composites are widely applied in various fields. It is reported that the incorporation of nanofillers increases the weight, brittleness, and opacity of materials. Nanocomposites are appropriate as high-performance applications that improve the overall properties of the final materials. Incorporating filler to a polymer matrix using nanosheet, due to its high contact surface and dispersion degree of nanosheets are important parameters in the materials' final properties. It is well known that the agglomerate tendency of nanosheets and form clusters is a challenge for the researcher to avoid this occurrence. The surface modification is an effective method to improve nanosheets stability and dispersion in various polymeric matrices. Plueddemann reported for the first time that silanes are suitable coupling agents. Later, Landmark studied the silanes and other coupling agents as surface modifiers for sheets and reported improvements in the sheets and polymer matrices' compatibility. Graphene is a suitable filler for significant improvement in mechanical, thermal conductivity, and electrical properties. However, the strong tendency of fillers towards aggregation and interfacial interaction are the main challenges in GNSs nanocomposites [3-7, 50]. Glass Flake (GF) has a laminated structure that can make a significant improvement in some physical and mechanical properties of plastics including shrinkage, dimensional stability, surface hardness, flexural stiffness, tensile strength, wear resistance. Incorporating glass flakes into coatings can exhibit good anticorrosive properties such as resistance to weathering, chemical attacks, abrasion resistance, low water vapor permeability, and fire retardant [8-11]. The presence of hydroxyl groups on the surface and edges of graphene nanoplatelets and the surface of GFs are suitable sites for reactions with silane coupling agents (VTMS). To confirm the functionalization of NGFs and GNPs, Fourier transforms infrared (FTIR) and energy-dispersive X-ray spectroscopy (EDX) was applied. To compare the influence of surface modification on the composites' physical and mechanical properties, tests such as water adsorption, dynamic mechanical-thermal analysis (DMTA), tensile, and three-point bending instruments were utilized.

2. Materials and Methods

2.1. Experimental & materials.

Nanoglass flakes (NGFs) with 350 nm thickness was provided by Glassflake Co. (England). Graphene nanoplatelets, commercially termed “xGnP-C750” with an average diameter of 2 μm and surface area of 750 m^2/g was obtained from XGSciences (USA). Epoxy vinyl-ester resin was supplied by Mokarar Chemical Co. (Iran). Potassium permanganate (KMnO_4), hydrogen peroxide (H_2O_2 , 30%), hydrochloric acid (HCl , 37%), and sodium nitrate (NaNO_3) were provided by Sigma-Aldrich. *N,N*-Dimethyl formamide, concentrated sulphuric acid (H_2SO_4 95-98%), acetone (99.7%) were purchased from Merck Chemical Co. Vinyl trimethoxy silane was provided by Dynasylan VTMO, Huls Chemical Co., Germany, in liquid form. MEK Peroxide was AKPEROX A60 purchased from Akpa Co. (Turkey), and cobalt naphthenate was obtained from Shimigaran Co. (Iran).

2.2. Preparation of graphene oxide.

Graphene oxide was prepared through the hummers method [10]. First, 1 g of GNS, 0.5 g of NaNO_3 and 30 mL of H_2SO_4 were mixed in an ice bath for a half hours, and then 3 g of KMnO_4 was slowly added into the solution. The ice bath was then eliminated, and the solution

was mixed with a magnetic stirrer for 8 h at room temperature. Then, the mixture temperature increased with the addition of 46 mL of deionized water, and it was refluxed for 30 min. The Termination reaction was carried out by adding a solution containing 30% hydrogen peroxide in deionized water and mixed for 10 min at room temperature. Finally, the product was washed with a solution of 10% HCl and deionized water until pH=7 was reached. The obtained graphene oxide was dried in a vacuum oven at 80 °C before use.

2.3. Functionalization of graphene oxide.

Graphene oxide surface modification was done by refluxing in a one-neck flask using a magnetic stirrer. At first, 1g of graphene oxide was dispersed in 50 mL DMF. Subsequently, 2 mL VTMS and 0.2 mL triethylamine were added to the flask. A magnetic stirrer stirred the mixture, and the reaction proceeded at 150 °C for 24 h, and at the end, the solution was centrifuged. Finally, to remove the solvent, the product was dried under a vacuum oven at 80 °C for 24 h.

2.4. Preparation of VE/GNS and VE/MGNS composites.

In brief, the preparation of the sample MGNS/VE was as follows: 1 g of MGNS was dispersed in 100 g of vinyl-ester resin by a high-speed mechanical mixer with (900 rpm) for 15 min at room temperature. Subsequently, an ultrasonic bath with a frequency of 37 kHz was applied for 45 min. Then, 0.5 % of cobalt naphthenate, 0.25% benzoin as a degassing agent, and 1% of MEKP were used as a curing agent. The sample GNS/VE was prepared using the same procedure.

2.5. Surface modification of NGFs.

NGFs surface modification was applied by the sol-gel method in a 500 mL one-neck flask, and it was refluxed under a magnetic stirrer. At first, 1 g of glass flakes was dispersed into acetone, and then 2 mL VTMS was added into the flask, and the reaction was continued at 60 °C for 24 h. To remove the unreacted VTMS, surface modified nanoglass flakes (MNGFs) were washed several times with acetone, and it was dried under a vacuum oven for 24 h at 60 °C.

2.6. Preparation of MNGFs/VE and NGFs/VE composites.

One gram MNGFs was dispersed in 100 g of epoxy vinyl-ester resin with a high-speed mechanical mixer at 500 rpm for 15 min. Consequently, the sample was sonicated for 45 min at room temperature under a frequency of 59 kHz. This resin's curing agents were 0.5% cobalt naphthenate, 0.25% benzoin as a degassing agent, and 1% MEKP used as a curing agent. The sample NGFs/VE was prepared in the same method.

2.7. Characterization techniques.

2.7.1. FTIR spectral studies.

Fourier transform infrared (FT-IR) measurement was applied to characterize functional groups of GNSs, MGNSs, NGFs and MNGFs according to the KBr technique by using a Bruker-IFS-48 FT-IR spectrometer (Ettlingen, Germany) in the range of 400-4000 cm⁻¹.

2.7.2. Scanning electron microscopy (SEM).

The SEM electron microscopes were performed to observe the dispersion of NGF and GNS before and after functionalization of the nanocomposites fractured surfaces. In order to avoid surface charging, The fracture surfaces were gold-coated before the SEM studies. The measurements were done on A VEGA/TESCAN scanning electron microscope with an accelerating voltage of 30 kV.

2.7.3. Water absorption.

The water uptake of the samples was measured according to ASTM D570-98. Specimens with 10 mm x 10 mm x 3.5 mm dimensions were used. Composite specimens were immersed in deionized water at room temperature for 36 days. The composite specimens were removed from the water and dried with a soft textile and then weighted by using an electronic balance at regular intervals. The values of the water absorption as percentages were calculated with the following Eq. (1):

$$\text{Absorption ratio: } W_a(t) = \frac{W_t - W_0}{W_0} \times 100$$

where $W_a(t)$ is the water absorption of the sample at time t , W_0 is the original weight, and W_t is the weight of the sample at a given immersion time t [28].

2.7.4. Mechanical testing.

The tensile tests were performed according to the ASTM D 638 procedure. The tensile properties were measured on a Santam material test system under a load cell at a crosshead speed of 5 mm/min at room temperature. The dimension of the tensile samples was 50 mm × 13 mm × 3.2 mm in the working section. The tensile test was employed to evaluate Tensile strength, tensile modulus, and strain. Flexural tests were carried out with a Santam machine at room temperature by following the ASTM D790 standard test method (three-point bending mode). Three-point bendings were used to determine the modulus of elasticity, flexural stress, and flexural strain values. The test was performed at a crosshead speed of 1.28 mm/min.

2.7.5. Dynamic mechanical, thermal analysis (DMTA).

DMTA studies of neat resin and its composites were performed on a Tritec 2000 DMTA dynamic mechanical, thermal analyzer. Samples were tested with dimensions of 10 mm × 5 mm × 2 mm under single cantilever mode. The scanning range varied from 0 °C to temperatures 180 °C of cured samples at a heating rate of 5 °C.min⁻¹ at the frequency of 1 Hz. The DMTA tests were carried out to analyze materials' viscoelastic properties, including modulus (G) factor (tanδ).

3. Results and Discussion

3.1. FT-IR analysis.

The FTIR transmittance spectra of the graphene and functionalized graphene nanosheets are illustrated in Fig. 1. It confirms the successful functionalization of graphene. Multiple characteristic peaks that have appeared in the 400-4000 cm⁻¹ range indicate silane groups' presence in the modified samples. The adsorption at 1004 cm⁻¹ and 1124 cm⁻¹ are

attributed to their respective C and Si-O-C stretching vibrations [12-14]. The new appeared peaks at 3443 and 3568 cm^{-1} , corresponding to hydroxyl groups on the graphene surfaces. This difference can explain the existence of major Si groups on graphene surfaces [15-16].

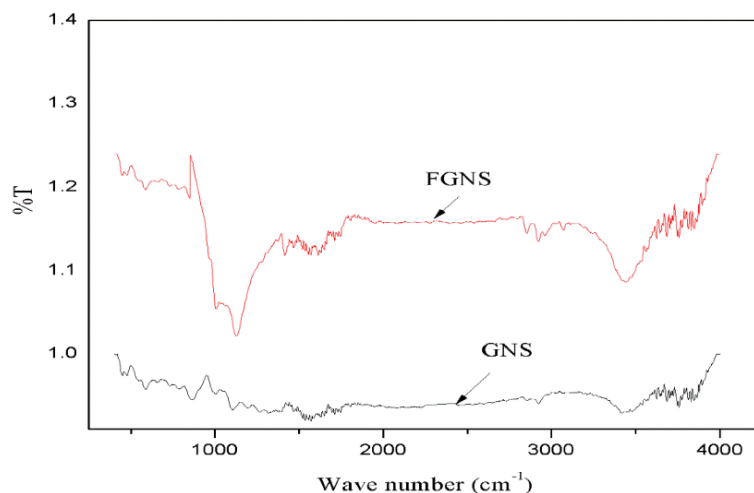


Figure 1. FTIR spectra of graphene and silane-modified graphene.

FTIR spectrum was performed to investigate the functionalization of nanoglass flakes shown in Fig. 2. In the case of treated flakes, three characteristic peaks were observed; two strong peaks at 1037 and 1102 cm^{-1} , which were attributed to Si-O-C and Si-O groups and hydrogen bonds forming between the hydroxyl groups on nano glass flake sheets [17].

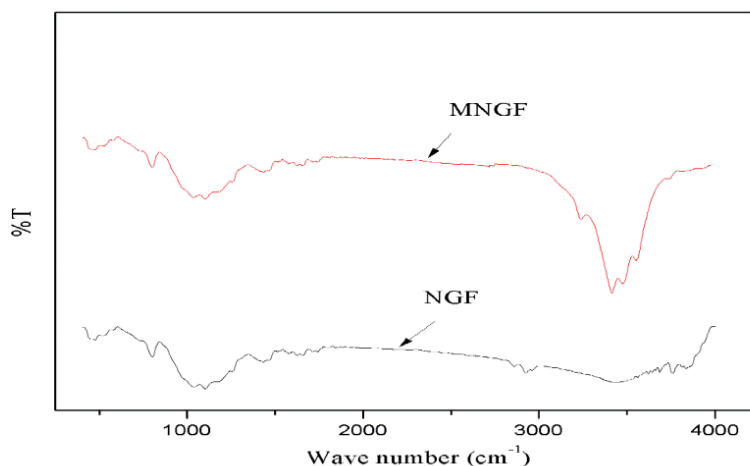


Figure 2. FT-IR spectra of nano glass flake and Modified nano glass flake.

3.2. Energy dispersive X-ray (EDX) analysis.

The elemental analysis of the functionalized GNSs and NGFs was characterized by energy-dispersive X-ray (EDX) analysis (Table 1.2).

Table 1. Elemental analysis of GNSs and MGNSs obtained from EDX.

Sample	C(%)	O(%)	Si(%)
GNS	96.94	3.06	-
MGNS	52.62	35.70	11.68

Table 2. Elemental analysis of NGFs and MNGFs obtained from EDX.

Sample	O(%)	Na(%)	Al(%)	Si(%)	k(%)	Ca(%)
NGFs	76.94	7.69	1.35	13.49	0.36	0.46
MNGFs	71.1	7.65	1.55	17.81	0.62	1.31

To obtain reliable results, the flakes with similar size and thickness were selected for EDX analysis. The elemental analyses of GNSs before and after functionalization were studied and shown in Table 1. The EDX results of graphene only show carbon and oxygen elements. In contrast, the elemental analysis of MGNS shows a new peak of the silicon atoms. Meanwhile, the percentage of the oxygen element in MGNS is stronger than that of GNS because many oxygen-containing groups were introduced due to the oxidation process. After the modification of GNS, a new peak of silicon appeared. The carbon ratio for both functionalization and non-functionalization in GNSs was fixed by 96.94% and 52.62%.

Furthermore, the oxygen percentage were managed by 3.06 and 35.70 percentages, respectively. The Si atom percentage of MGNSs was 11.68, concluding that graphene oxide nanosheets successfully modified silane molecules. The EDX elemental analysis of NGF and MNGFs represented O, Na, Al, Si, K, and Ca atoms. The results unveiled that after modification of the surface of NGF the Si concentration increased. Si's atomic ratio was enhanced by about 32% after modification, but the percentage of oxygen was dropped by about 8%. The ratios of other atoms are almost identical, as shown in Table 2. The decreased percentage of oxygen was attributed to many oxygen-containing groups cleaved by silane groups. Hence, the result of EDX analysis clearly proved that VTMS molecules were successfully attached to GNSs and NGFs flakes and confirmed FTIR transmittance spectra results.

3.3. Morphological studies.

SEM was utilized to evaluate the morphology and structure of GNS/VE and NGFs/VE composites before and after the functionalization process [18]. The SEM image of GNSs/VE composite in Fig. 3a shows that some untreated graphene platelets are heavily agglomerated. The structure appears “fluffy”, as reported in [18-19]. In contrast, a clear distribution of graphene sheets was achieved after oxidation and silane modification. There was no MGNS cluster evident in the cross-section shown in Fig. 3b. The enhanced dispersion and interfacial bonding were due to covalent bonding between the vinyl-ester and the VTMS molecules grafted on the GNSs surface [20-21]. Figs. 3c, 3d show the SEM images NGFs/VE and MNGFs composites. The result shows nanoglass flakes are well dispersed in vinyl-ester without agglomeration. The bright zones on the black area could be related to MNGFs[22]. The fracture surface exhibits good adhesion and compatibility with the matrix due to its surface treatment [23]. Though nanosheets have shown quite smooth distribution in GNSs and NGFs surface modifications, graphene sheets exhibit more homogeneously dispersed than nanoglass flakes in the vinyl-ester matrix.

3.4. Water absorption.

To evaluate the influence of fillers' water barrier properties, water absorption of nanocomposites was measured. Fig. 4 shows water absorption versus time profile for neat, NGFs, MNGFs, GNSs, and MGNSs composites under the same condition. The absorption ratio indicates the amount of water absorption by the nanocomposites [24]. The composites show a rapid water uptake within the initial 72 h. This phenomenon can explain as a lie in the first stage of the absorption process in the nanocomposite component. The uptake of a larger amount of water can be described by interrupting processes or slow deformation. Then, slow growth in

the percentage of absorption was observed in 360 h, and it continued till the end of testing time [25-26].

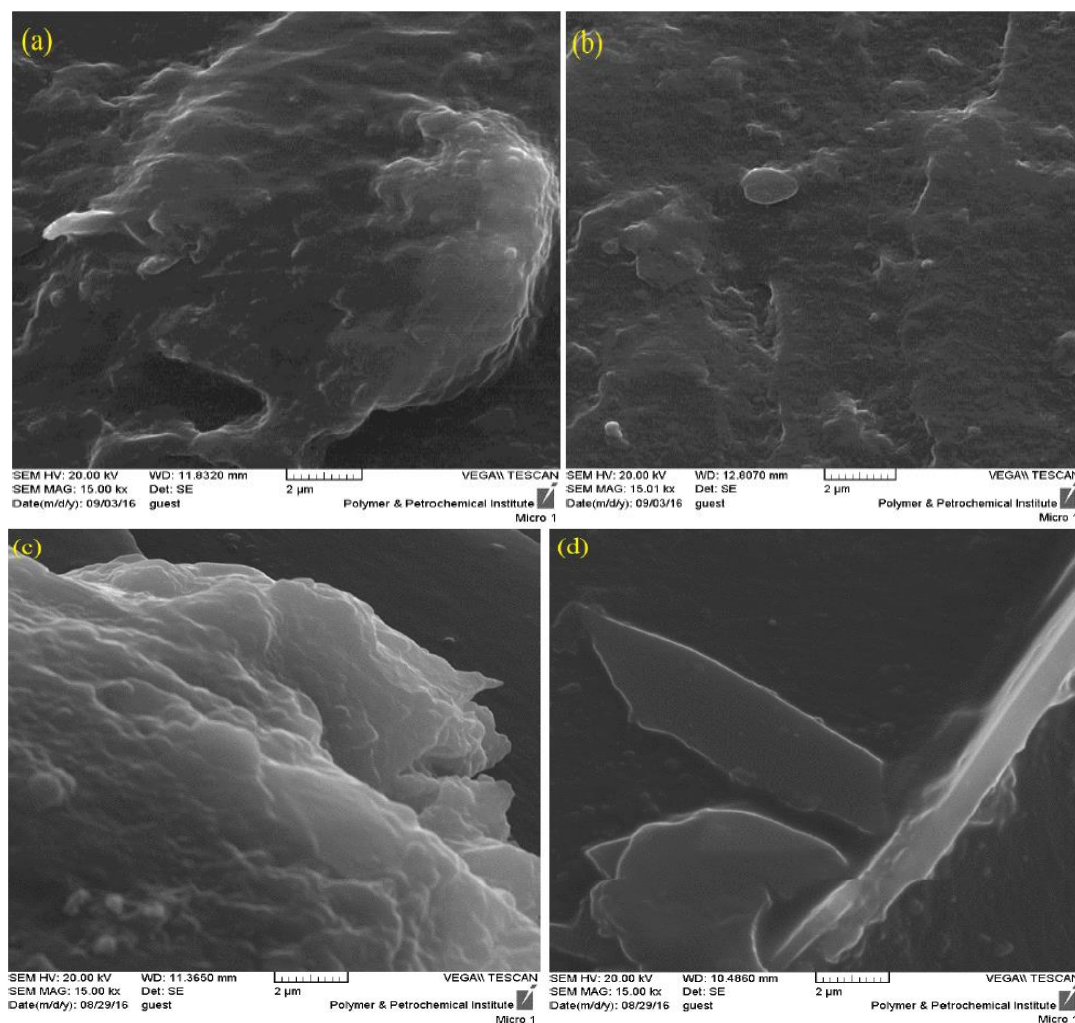


Figure 3. SEM images of the fractured sections of (a) VE/GNS, (b) VE/MGNS, (c) VE/NGFs, (d) VE/MNGFs composites.

Results exhibited the water absorption of treated samples was lower than untreated and neat resin. The water adsorption in the first 24 h of the functionalized GNSs compared to that of non-functionalized was almost 28%. Compared to the neat resin, it was about 41%. The absorption of untreated GNSs composites was 22% lower than that of neat resin. In the case of glass flakes, water absorption was decreased even more compared to GNS composite. The surface-treated NGFs absorbed almost 31%, less than untreated NGFs. Compared to neat resin, the incorporation of MNGFs reduced water absorption to half the value of neat resin. In continuation, this trend was maintained in VE/MNGFs composite and untreated NGFs with 27% uptake lower than neat resin. As shown in Fig. 4, the water absorption of GNSs composite was almost 18% higher than MNGFs/VE composites.

Moreover, we found that the maximum absorption ratio was obtained during absorption testing, which was 1.23 mass% for neat resin and 0.96 and 0.91 mass% for GNSs and NGFs composites. The data shows that modified nanoflakes lowered the diffusion and increased the amount of uptake water in the composites, which was less than the unmodified composites and neat resin. The water barrier properties improvement in modified composites is due to improved filler dispersion in modified composites and present hydrophobic groups on nanosheets' surface. The obtained results represent that the functionalization of GNSs and

NGFs, which may limit water absorption in the composites. However, MNGFs composites represent better barrier properties than MGNSs composites. Absorption of GNSs composites takes place more rapidly as the sheet thickness is smaller than NGFs samples. This may create some spaces between smaller nanosheets called “free” or “interstitial volume” which can accommodate additional water by capillary action. The bigger in interstitial volume per unit mass of absorbent, the higher would be the ultimate degree of absorption. Another reason for the lower absorption rate of MNGFs and NGFs samples may be attributed to composites' unsaturation containing more significant size filler. The interstitial volume is smaller with decreasing sheet size, but the water absorption for MGNS composites is saturated [26, 27]. The nanosheets morphology could affect fractional free volume. The tortuous diffusion path leads to a change in the permeability of nanocomposites. The improvement in water barrier properties of NGFs composites suggests stronger polymer/filler interaction and causing increased hydrophobicity due to a higher ratio of silane molecules present on the surface of MNGF than MGNS, resulting, the water molecules encounter in the more tortuous pathway for travel through the composites. Since the presence of layered NGFs caused immobilized chain segments and decreased free volume. As a consequence, the water permeability coefficient is reduced [28].

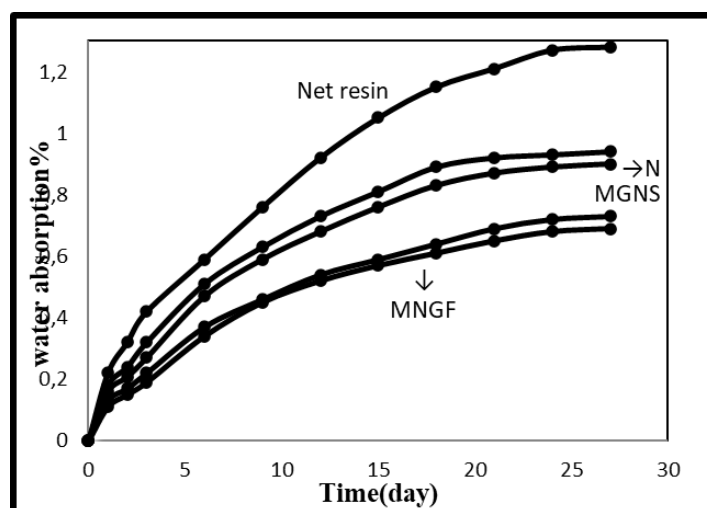


Figure 4. Water absorption behavior of neat resin, MNGFs/VE, NGFs/VE, MGNSs/VE, GNSs/VE composite.

3.5. Mechanical properties.

Tensile testing was carried out to investigate and compare GNSs and NGFs treatments' influence on composites' mechanical behavior. The obtained stress-strain curves are exhibited in Fig. 5. Important tensile properties are listed in Table 3. The nanocomposite containing unmodified NGFs tends to reduce tensile strength and Young's modulus. In contrast, the addition of MNGFs has the opposite effect. It was found that the tensile strength of NGFs and elongation-at-break and modulus were reduced compared with neat resin. In treated cases, the NGF nanocomposite tensile strength, elongation-at-break were increased by about 175% and 110%, respectively, compared with untreated NGFs/VE composite. The MNGFs/VE composite has exhibited 57% improvement in tensile strength, 70% for elongation-at-break than neat resin. The decreased elongation-at-break of the samples indicates that nano glass flakes were limited the macromolecular mobility to some extent, as reported before[30]. It has been established that the microstructure of samples mainly affects the physical and mechanical properties of nanocomposites. The free volume cavities and concentration depend on filler and

chain morphology, i.e., they depend on chain slippage under the external forces. Another reason may be the localization of the layered plates of glass flakes between polymer chains, reducing entanglements and -link density, decreasing the sample's strength [8,22]. As shown in Fig. 5, incorporating GNSs to vinyl-ester composite improves the tensile strength by about 10%, and elongation-at-break was slightly decreased than neat resin. In comparison, MGNSs/VE and GNSs/VE composites tensile strength, elongation-at-break, and Young's modulus were enhanced by 60%, 46% and 22%, and compared to neat resin, they were enhanced by 76%, 42%, 27%, respectively. This is attributed to interactions between polymer and filler in the system [31]. GNS/VE composite exhibits 93%, 20%, and 10% higher tensile strength, elongation-at-break, and modulus than NGFs/VE composite, in the stated order. Although both modified and unmodified nanosheets can exhibit higher tensile strength and elongation-at-break than neat resin [32]. As can be seen from Fig. 5, incorporation of GNSs to vinyl-ester improved composite tensile strength. However, elongation-at-break was slightly decreased than the neat resin. This is attributed to interface interactions and adhesion of matrix and filler in the composites [31]. Although modified and unmodified nanosheets can impart higher tensile strength and elongation-at-break than neat resin [32]. The Young modulus was also increased in both treated and untreated GNS composite in comparison with neat resin. These results indicate that untreated graphene represents stronger interaction with the polymeric matrix in comparison with untreated NGF. By comparison, the composites containing the functionalized MNGFs represent higher tensile strength and elongation-at-break values than other nanocomposites. The presence of graphene and glass flakes results in a greater hindering effect and less flexibility and motion of the chains. Eventually, it causes strain-at-break to reduce slightly [8]. We have found that the incorporation of MGNSs, overall, made the biggest improvement in modulus and tensile strength. However, MNGFs show the highest elongation-at-break in comparison to MGNSs/VE composite. The differences in NGF and GNS composites' mechanical properties are attributed to different surface properties and size sheets [33-34]. The untreated filler tends to agglomerate in the matrix, and agglomerated fillers act as a stress point, which leads to reduced tensile strength [29]. The presence of glass flakes leads to decrease strength by reduction of entanglements, chain motion, and prevention of oriented chains. However, after modification, the interactions between graphene, polymer, and glass flake polymer chains are enhanced. The incremental rate of the modulus in the nanocomposite of NGF is lower than GNS nanocomposites. Therefore, slippage of glass flakes may occur during extension and spoil the reinforcement potential of nanofillers. There have been four scenarios proposed for taking nanofillers in a polymeric matrix that summarized below. 1. Separate standing of each nanolayer in the matrix; 2. Contact in filler edges with each other 3. Overlapping of some parts of nanolayers on each other; 4. Complete placement of nanolayers on each other [8]. From the mechanical properties, the lower mechanical properties of untreated sample may occur due to various reasons such as contacting of filler edges, overlapping each other more closely and tightly, or complete adjustments of nanolayers on each other, which lead to decreased filler dispersion and surface contact of polymer with filler and more slippage of a polymer chain. Another reason for variation in tensile strength is due to free volume. In other words, when free volume content decreases, the tensile strength increases. The reduction in free volume increases the tensile strength with increased dispersion of modified fillers, which may suggest good interaction between the filler and matrix provided by a silane coupling agent. From the above discussion, it is evident that enhancement in mechanical properties in GNS-filled composites is higher than NGF filled samples. The NGF

with a larger size has less aspect ratio than GNS. Therefore, it is evident that for fillers with bigger sizes, the aspect ratio had an insignificant effect on enhancing mechanical properties. Therefore, the significant improvement of mechanical properties is related to the enhancement of MNGF and MGNS dispersion and refers to the improved adhesion between the fillers and the polymer host, which results in efficient load transfer between filler and polymer. The results due to substantial hindrance effect that caused limited chain mobility and flexibility ultimately reduce the strain-at-break significantly [8, 29, 51].

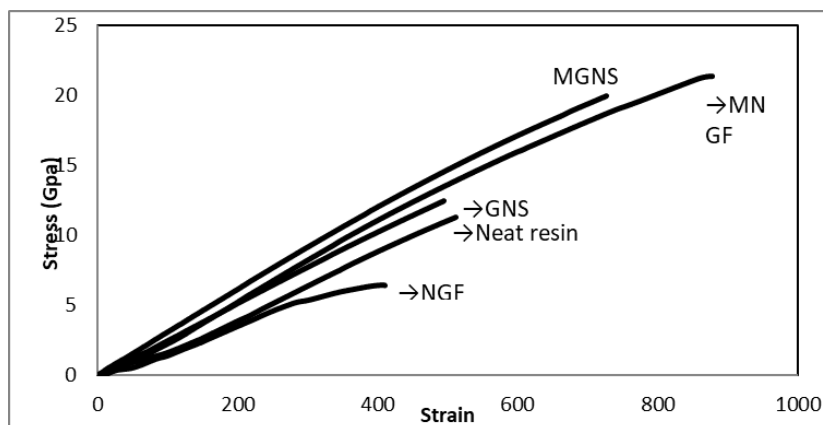


Figure 5. Tensile stress versus strain of neat VE, GNS/VE, MGNS/VE, NGFs/VE, and MNGFs/VE composites.

Table 3. Mechanical properties from tensile testing for NGFs/VE, GNSs/VE before and after functionalization, and neat composites.

Sample	Tensile strength(MPa)	Elongation at break(%)	Young's modulus (MPa)
Neat resin	11.33	1.39	20.5
NGF	6.46	1.12	17.6
MNGF	17.78	2.37	23.8
GNS	12.50	1.35	23.7
MGNS	19.93	1.97	30.1

The three-point bending is a flexural test employed to test the mixture's compressive and tensile forces likely encountered in the normal state of nanocomposites. This analysis was performed to evaluate how modified flakes' incorporation affects the vinyl-ester matrix's mechanical properties. Fig. 6 shows the flexural strain-stress curve for neat vinyl-ester and composites. The results are summarized in Table 4. Incorporation MNGFs exhibit higher flexural strength and flexural modulus of the vinyl-ester matrix than the NGFs/VE composite. In MGNSs, the flexural strength and flexural modulus are enhanced almost by 106%, and 56%, and elongation-at-break was improved after modification of graphene nanosheets. By comparison, MGNSs flexural modulus was up by 1.2 GPa, which is higher than MNGFs, and their flexural strength was increased. Nanoscale surface roughness and wrinkled structure of GNS enhance mechanical interlocking caused to improve adhesion [30]. GNS has a smaller thickness than NGF. It displays a higher specific surface area, and the specific surface area plays an important role in micromechanical models such as the Halpin–Tsai model. In Hese models, the higher specific surface area and higher filer modulus lead to improved effective load transfer from the matrix to nanofillers, caused to the increased modulus. [35, 36]. The covalent bonding may be formed between the vinyl-ester matrix and the silane functional group on NGF and GNS, further improving the interfacial bonding leading to mechanical bonding[30]. In general, there is a strong argument over the influence of filler size on the flexural strength of the surface-treated composite, as some studies report that the flexural strength is decreased when composites are filled by larger size nanoparticles [37]. Two factors

should be described: the proper dispersion of the nanoparticles and the interfacial adhesion in the composites.

Regarding the first factor, there are more agglomerates in composites, which may cause embrittlement effects. Large agglomerates in the matrix lead propagated cracks and induce the final failure. The presence of rigid fillers in the matrix leads to brittle behavior in composite, which is reflected as reduced elongation-at-break of the materials. Two reasons explain the enhancement in flexural strength and modulus of the MGNS and MNGF composites. First, strong covalent bonding between nanofillers and matrix required improved dispersion of the flakes layers through the matrix and improved composites' mechanical properties [38-39]. This indicates the effect of the homogeneous distribution of nanoflakes within the matrix. As explained earlier, the second reason attributed to the polymer-filler interaction of composites plays an essential role in improving the mechanical properties. Stress transfer capability and elastic deformation from the matrix to fillers are governed by a strong bonding between nanoparticle and matrix [37].

Table 4. Flexural properties from three-point bending for NGFs/VE, GNSs/VE before and after functionalization, and neat composites.

Sample	Elongation-at-break(%)	Flexural strength (MPa)	Flexural modulus (MPa)
Neat resin	4.04	15.84	1015.86
NGF/VER	5.38	15.72	756.41
MNGF/VER	4.94	19.72	1011.14
GNS/VER	4.74	14.53	791.34
MGNS/VER	6.78	29.95	1236.22

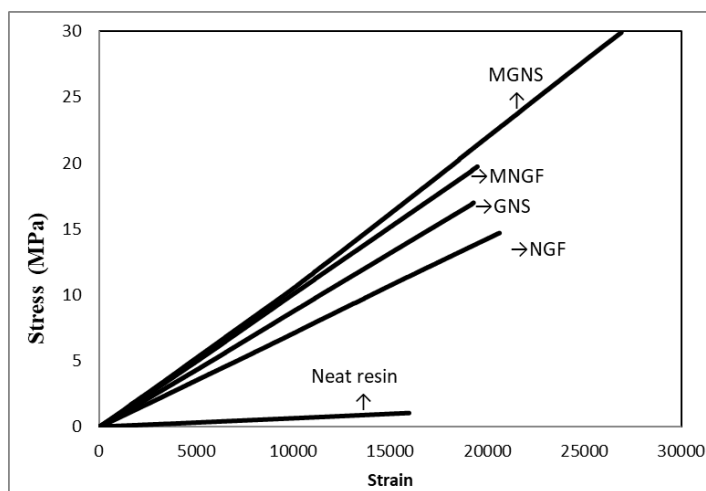


Figure 6. Typical flexural strength versus strain curves for neat resin and composites containing NGF, MNGF, GNS, MGNS.

3.6. Dynamic mechanical, thermal analysis of the samples (DMTA).

DMTA characterizes the storage modulus and tan delta (loss factor) of nanocomposites in the temperature range of 50-180 °C. Glass transition temperature is defined as changes in a slope of storage modulus transition or maximum in tan δ curve. Fig. 7 exhibits glass transition temperature leads to increased chain mobility at the alpha (α) transition [40]. For neat VE, tan δ peak is observed around 117 °C by incorporation of unmodified GNS and NGF and T_g is slightly decreased to 114 and 113 °C. However, after modification GNS and NGF T_g s were 129 and 122 °C respectively.

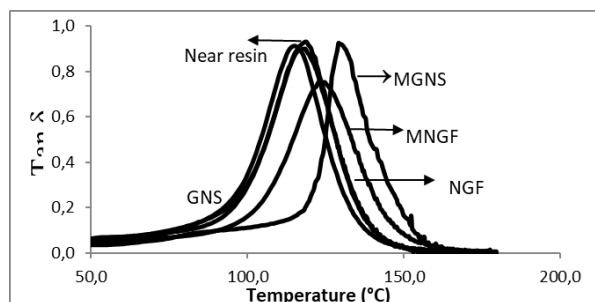


Figure 7. Damping behavior of neat vinyl-ester and GNS/VE, NGF/VE, MGNS/VE, MNGF/VE composites.

The presence of nanofillers could affect molecular dynamics. The T_g temperature depends on surface features, dimensions, symmetry, etc. The glass transition temperature has increased in modified nanocomposites in comparison with neat resin and also unmodified nanocomposites. This increment can be due to the restriction of chain mobility in the interphase region. This is more evident in MGNS than MNGF samples due to the difference in quantity and quality of interface region in nanocomposites. The greater quantity of GNS interphase region in nanocomposites is the understandable cause of the larger surface area of smaller-sized filler, leading to higher T_g shift in MGNS samples[41]. Improvement in the interaction between matrix and nanofillers helped to increase the glass transition temperature of the sample. The surface modification of graphene and glass flake can prevent polymer chain mobility on the surface of nanofillers. Sheet size, dispersion, surface modification of fillers, and interfacial adhesion with polymer play essential roles in T_g change [36]. The results display an eminent influence of interface in thermal features of the VE/GNS and VE/NGF composites.

On the other hand, the height of $\tan \delta$ decreased drastically after modifying the nano glass flakes. This result may suggest that the macromolecules are strongly bound to NGFs. The change in the height of $\tan \delta$ peak is related to the matrix chains' relaxation process in these nanocomposites. Reflection on improved interaction between vinyl-ester resin and NGFs may be related to the existing higher ratio of silane modifier on MNGF surface than MGNS [42]. Fig. 8 shows temperature dependency in the storage modulus of neat VE resin and its nanocomposites. All composites exhibited higher storage modulus (E') than a neat vinyl ester. The enhancement in E' values by adding modified nanosheets exhibited the material features to store energy due to reinforcement properties and limitation of matrix chain motion upon GNS incorporation. Storage modulus corresponding to materials' capability to store the energy is one of the important parameters in DMTA measurements [40]. For both nanocomposites, nanofillers' incorporation caused increased storage modulus in the wide range of temperature, from glassy to rubbery region. As temperature rises, the chains turn into a rubbery state, and the storage modulus decreased. From the investigated results, clear the filler's presence will be more intensified this behavior [43].

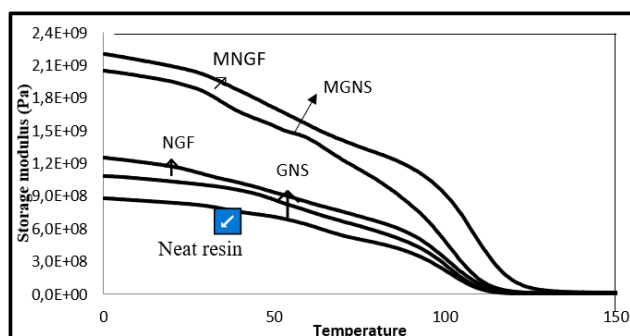


Figure 8. Storage modulus behavior of neat vinyl-ester and its composites before and after functionalization.

Although it's conspicuous that the storage modulus at the glassy region is higher than the rubbery region [44]. The vinyl ester's storage modulus is improved significantly by incorporating a graphene sheet and glass flake nanosheets. The value of storage modulus composites filled with a GNS and NGF is observed to be 23% and 42% (2061.6 MPa) higher than (1843.1 MPa) of the cured neat vinyl ester. The NGF composite was slightly improved than the non-functionalized GNS composite within a glassy state (at 0 °C). Compared to NGF, the GNS composite exhibits lower storage modulus, which may correspond to VE/GNS composite is less rigid than VE/NGF composite [40]. More storage modulus improvement is obtained in MGNS and MNGF composite, approximately 131% and 149% compared with neat resin. This result indicates that VE/MNGF samples' stiffness is at the highest value among all the examined samples [45].

Furthermore, the nanocomposite storage modulus with MGNS is 2.049 GPa, much higher than unmodified graphene composite (about 88%). The increase in the composites' storage modulus is more pronounced in MGNS and MNGF-based vinyl-ester than the untreated and neat resin. The results again illustrate the reinforcement effect of the silane modification on GNS and NGF sheets. The reductions in the local chain's motion around the sheets are due to the improved interfacial interactions and dispersion of nanosheets in the vinyl-ester matrix [19, 35, 45-49].

3.7. Molecular dynamics simulations of graphite-vinyl-ester nanocomposites.

Based on our previous works [52-108], the effects of geometrical data on mechanical characterizes of graphite-vinyl-ester Nanocomposites are investigated using molecular dynamics (MD) and Monte-Carlo simulations by Charmm software. Graphite hexagonal crystal group is modeled (Fig. 9), and molecular dynamic geometry data, such as periodic cell size and several layers, are simulated for studying their effect on graphene orients related to mechanical behavior. NVT (stands for a constant number of atoms, volume, and temperature) is the thermodynamic ensemble used via the entire simulation. Dynamic time for atomic modeled is proportional to the number of units included in each supercell. A dynamic step of 0.1 fs with simulation temperature equal=300 including 95 kcal/mol energy deviation, was done using Hyper-Chemistry software (Fig.9) .

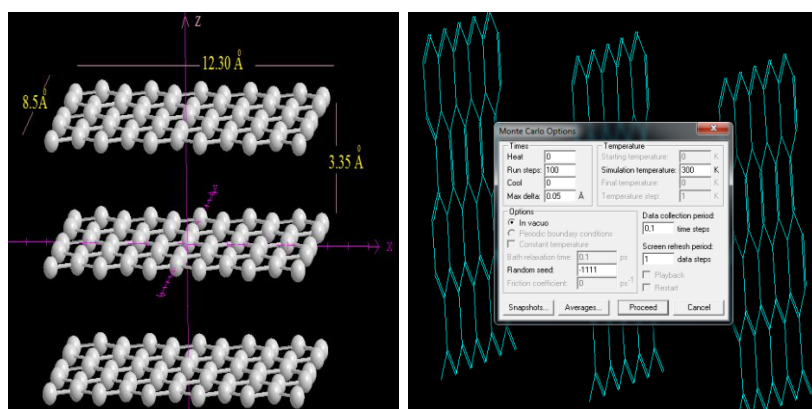


Figure 9. Graphite hexagonal crystal group with 3 layers and Montecarlo simulation.

Graphene Lee *et al.* [109]. Reported a Young's modulus of 1.0 TPa, and suitable strength of 130 GPa measured via Nano-indentation atomic forces microscope for each layer [109]. Additionally, Graphene nanocomposites are envisaged to make enhanced entirely mechanical properties. Exfoliated graphite Nano-layers are new types of Nano-particles,

including graphene stacks of 5~10 nm thickness. Exfoliated graphene Nanosheets share chemical structures with carbon nanotubes (CNT). Their edges could be easily modified chemically for dispersion enhancement in polymeric composites. Fig. 3 exhibits the morphology of SEM images of the fractured sections of VE/GNS, VE/MGNS, VE/NGFs, and VE/MNGFs composites compared with MD. Vinyl-ester resin (VER), is a resin produced by the esterification of an epoxy resin with acrylic or methacrylic acids. The "vinyl" groups refer to these ester substituents, which are prone to polymerize. The diester product is then dissolved in a reactive solvent, such as styrene, to approximately 30–46 percent content by weight (Figs.10,11).

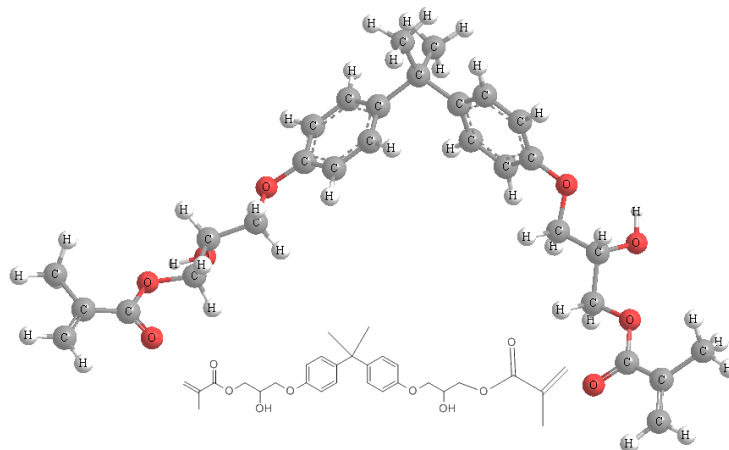


Figure 10. Geometry optimization “vinyl ester” via abinitio calculation.

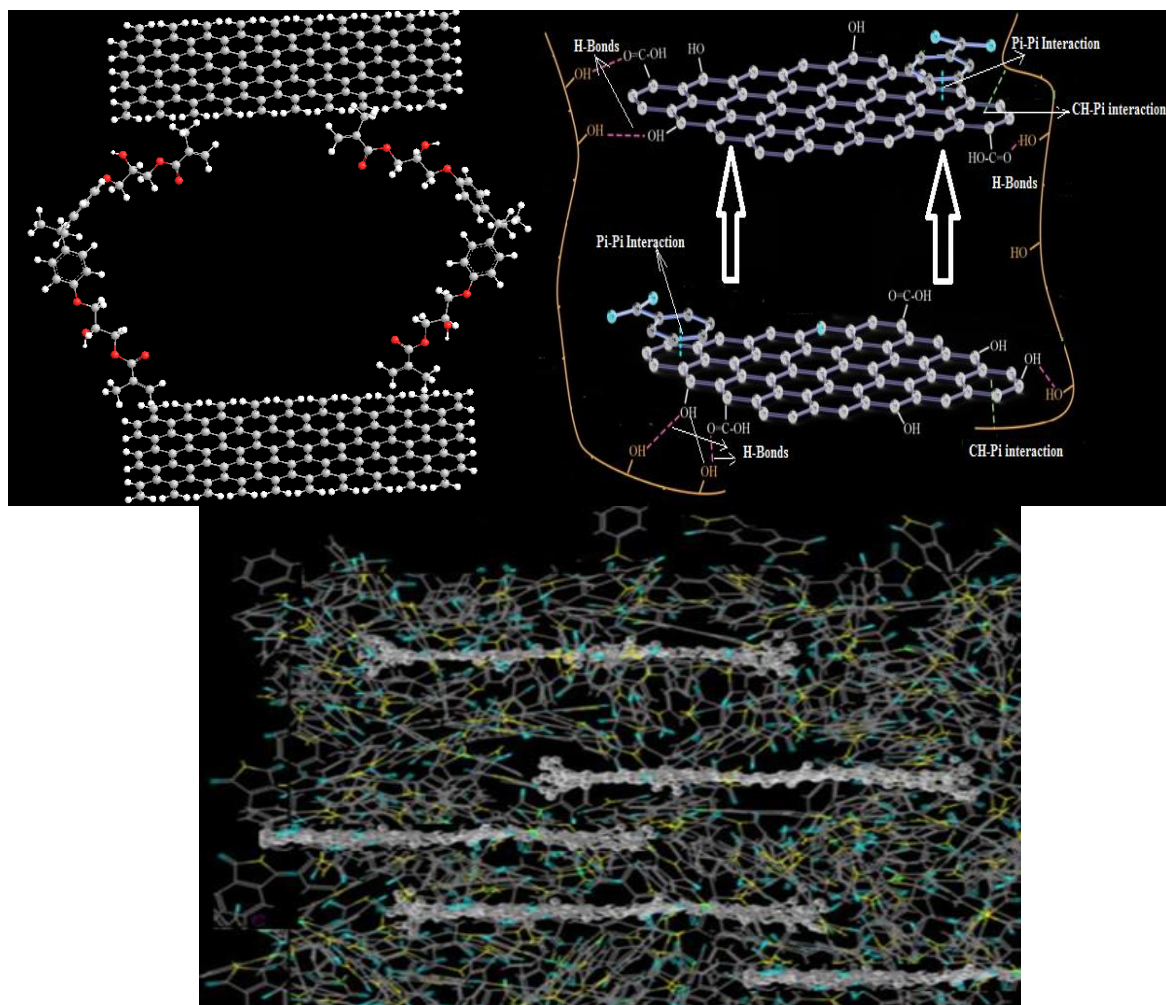


Figure 11. Simulation of non-covalently functionalized-graphene interaction by Vinyl-ester resin

Those simulated nanosheets are generally around 5 nm thick. They can be synthesized via lateral dimensions ranging from less than 5 μm to up to a hundred μm . Vinyl-ester is a copolymer thermoset resin produced via the esterification of an epoxy resin with unsaturated mono-carboxylic acid. This reaction is then dissolved into the reactive solvent, such as styrene. Vinyl-ester is an important polyester alternative and epoxy material in the matrix or composite material. Its distinctive properties, strength, and bulk cost lie intermediately between polyester and epoxy. It has low resin viscosity, less than polyester and epoxy [109,110]. Although the epoxy-based vinyl-ester resin has considerable corrosion resistance, understanding physical properties is important due to their chemical composition and the presence of polar hydroxyl. Simulated vinyl-ester chains are 60% epoxy, and 40% styrene produces an ideal vinyl-ester chemical chain assuming that all the epoxy had reacted.

Although Vinyl-ester-resin has low resistance for cracking propagation or brittleness and shrinkage during polymerization, the synthesized nanoparticles' methods into a resin solution process can remove this problem. Since the interaction among the nanoparticles with the matrix is van der Waals force, the in-situ synthesis manner can be creating stronger chemical bonding within the composite (Fig.11).

Based on MD discussion (for pristine graphene and graphene oxide), interfacial shear strength resulting from the molecular dynamic (MD) simulations for PG-vinyl-ester and GO-vinyl-ester should be stronger than vinyl-ester.

4. Conclusions

This study has investigated and compared the influence of GNS and NGF functionalization and dispersion on the physical and mechanical properties of vinyl-ester nanocomposites. Various characterizations, including FTIR, EDX, and results, demonstrate that VTMS coupling agents successfully treated graphene oxide and NGF sheets' surface. The analysis of the GNS and NGF with EDX demonstrates that there are more oxygen and Si functional groups exist on the NGF compared with GNS. However, GNS shows a greater increase in Si group after functionalization than NGF. SEM results show better dispersion and distribution of GNS and NGF in the vinyl-ester matrix obtained after functionalizing the nanosheets. Composites containing modified nanosheets exhibited lower water absorption than untreated samples due to better dispersion and hydrophobic groups' presence on the surface of nanosheets. MNGF/VER composite shows lower water absorption compared with MGNS/VER. This result is probably an indication of the hydrophilic group on graphene surfaces. It is found that the functionalized GNS and NGF has resulted in higher tensile strength, flexural modulus, and elongation-at-break of vinyl-ester resin compared with unfunctionalized and neat resin. MGNS/VER composite has exhibited further tensile strength and flexural modulus than MNGF/VER composite. However, MNGF/VER shows better elongation-at-break than MGNS/VER. The DMTA results exhibited increased storage modulus and decreased T_g by incorporation NGF and GNS. Nonetheless, the incorporation of functionalized graphene nanosheets and nanoglass flakes represent higher T_g and storage modulus. MNGF/VER presents more storage energy compared with MGNS/VER composites. MD simulations prove that exfoliation improves the mechanical properties of graphite nanoplatelet vinyl-ester nanocomposites. MD simulation revealed that, although there is minimal effect of pure vinyl ester, it tends to enhance interfacial shear strength between PG-vinyl-ester and GO-vinyl-ester in a considerable magnitude.

Funding

This project has funded by Iran Polymer and Petrochemical Institute

Acknowledgments

The authors would like to thank the Iran Polymer and Petrochemical Institute for funding the current project. The authors also would like to extend the acknowledgments to Mokarrar chemical Inc. for providing vinyl-ester resin for this work.

Conflicts of Interest

The authors declare no conflict of interest.

References

1. Ehsani, M.; Khonakdar, H.A.; Ghadami, A. Assessment of morphological, thermal, and viscoelastic properties of epoxy vinyl-ester coating composites: Role of glass flake and mixing method. *Progress in Organic Coatings* **2013**, *76*, 238-243, <https://doi.org/10.1016/j.porgcoat.2012.09.010>.
2. Quintanilla, A.L. *Fundamentals of Particulate-Filled Polymer Composite Fabrication via Continuous Liquid Interface Production (CLIP)*. North Carolina State University; **2017**.
3. Zhang, X.; Bitaraf, V.; Wei, S.; Guo, Z.; Zhang, X.; Wei, S.; Colorado, H.A. Vinyl-ester resin: Rheological behaviors, curing kinetics, thermomechanical, and tensile properties. *AIChE Journal* **2014**, *60*, 266-274.
4. Kuilla, T.; Bhadra, S.; Yao, D.; Kim, N.H.; Bose, S.; Lee, J.H. Recent advances in graphene based polymer composites. *Progress in Polymer Science* **2010**, *35*, 1350-1375, <https://doi.org/10.1016/j.progpolymsci.2010.07.005>.
5. Pavlidou, S.; Papaspyrides, C.D. A review on polymer-layered silicate nanocomposites. *Progress in Polymer Science* **2008**, *33*, 1119-1198, <https://doi.org/10.1016/j.progpolymsci.2008.07.008>.
6. Chirita, G.; Dima, D.; Andrei, G.; Birsan, I. Mechanical Characterization of Graphite and Graphene / Vinyl-Ester Nanocomposite Using Three Point Bending Test. *Materiale Plastice* **2016**, *53*.
7. Abedalwafa, M.; Wang, F.; Wang, L.; Li, C. Biodegradable poly-epsilon-caprolactone (PCL) for tissue engineering applications: A review. *Reviews on Advanced Materials Science* **2012**, *34*, 123-140.
8. Ghadami, A.; Ehsani, M.; Khonakdar, H.A. Interrelationship of thermal and mechanical properties of poly(ethylene terephthalate)/poly(ethylene 2,6-naphthalate)/graphene nanocomposites. *Journal of Vinyl and Additive Technology* **2017**, *23*, 210-218.
9. Broughton, W.R.; Lodeiro, M.J.; Pilkington, G.D. Influence of coupling agents on material behaviour of glass flake reinforced polypropylene. *Composites Part A: Applied Science and Manufacturing* **2010**, *41*, 506-514, <https://doi.org/10.1016/j.compositesa.2009.12.007>.
10. Ghadami, A.; Ehsani, M.; Khonakdar, H.A. Vinyl ester/ glass flake nanocomposites: An overview of chemical and physical properties. *Journal of Composite Materials* **2013**, *48*, 1585-1593, <https://doi.org/10.1177/0021998313488153>.
11. Wang, G.; Yang, J. Influences of glass flakes on fire protection and water resistance of waterborne intumescent fire resistive coating for steel structure. *Progress in Organic Coatings* **2011**, *70*, 150-156, <https://doi.org/10.1016/j.porgcoat.2010.10.007>.
12. Venkateswara Rao, A.; Lathe, S.S.; Nadargi, D.Y.; Hirashima, H.; Ganesan, V. Preparation of MTMS based transparent superhydrophobic silica films by sol-gel method. *Journal of Colloid and Interface Science* **2009**, *332*, 484-490, <https://doi.org/10.1016/j.jcis.2009.01.012>.
13. Ma, W.-S.; Li, J.; Deng, B.-J.; Zhao, X.-S. Preparation and characterization of long-chain alkyl silane-functionalized graphene film. *Journal of Materials Science* **2013**, *48*, 156-161, <https://doi.org/10.1007/s10853-012-6723-5>.
14. Lee, C.Y.; Bae, J.-H.; Kim, T.-Y.; Chang, S.-H.; Kim, S.Y. Using silane-functionalized graphene oxides for enhancing the interfacial bonding strength of carbon/epoxy composites. *Composites Part A: Applied Science and Manufacturing* **2015**, *75*, 11-17, <https://doi.org/10.1016/j.compositesa.2015.04.013>.
15. Wang, J.; Xu, C.; Hu, H.; Wan, L.; Chen, R.; Zheng, H.; Liu, F.; Zhang, M.; Shang, X.; Wang, X. Synthesis, mechanical, and barrier properties of LDPE/graphene nanocomposites using vinyl triethoxysilane as a coupling agent. *Journal of Nanoparticle Research* **2011**, *13*, 869-878, <https://doi.org/10.1007/s11051-010-0088-y>.
16. Mohandes, F.; Salavati-Niasari, M. Freeze-drying synthesis, characterization and in vitro bioactivity of chitosan/graphene oxide/hydroxyapatite nanocomposite. *RSC Advances* **2014**, *4*, 25993-26001, <https://doi.org/10.1039/C4RA03534H>.

17. Hu, X.; Su, E.; Zhu, B.; Jia, J.; Yao, P.; Bai, Y. Preparation of silanized graphene/poly(methyl methacrylate) nanocomposites in situ copolymerization and its mechanical properties. *Composites Science and Technology* **2014**, *97*, 6-11, <https://doi.org/10.1016/j.compscitech.2014.03.019>.
18. Ghadami, A.; Ehsani, M.; Khonakdar, H.A. A comprehensive study on morphological and rheological behavior of poly(ethylene terephthalate) and poly(ethylene-2,6-naphthalene) nanocomposite blends in presence of graphene. *Journal of Vinyl and Additive Technology* **2017**, *23*, E160-E169.
19. Ramanathan, T.; Stankovich, S.; Dikin, D.A.; Liu, H.; Shen, H.; Nguyen, S.T.; Brinson, L.C. Graphitic nanofillers in PMMA nanocomposites—An investigation of particle size and dispersion and their influence on nanocomposite properties. *Journal of Polymer Science Part B: Polymer Physics* **2007**, *45*, 2097-2112.
20. Wan, Y.-J.; Gong, L.-X.; Tang, L.-C.; Wu, L.-B.; Jiang, J.-X. Mechanical properties of epoxy composites filled with silane-functionalized graphene oxide. *Composites Part A: Applied Science and Manufacturing* **2014**, *64*, 79-89, <https://doi.org/10.1016/j.compositesa.2014.04.023>.
21. Kathi, J.; Rhee, K.Y. Surface modification of multi-walled carbon nanotubes using 3-aminopropyltriethoxysilane. *Journal of Materials Science* **2008**, *43*, 33-37, <https://doi.org/10.1007/s10853-007-2209-2>.
22. Salehi, S.; Ehsani, M.; Khonakdar, H. Assessment of thermal, morphological, and mechanical properties of poly(methyl methacrylate)/glass flake composites. *Journal of Vinyl and Additive Technology* **2015**, *23*, 62-9.
23. Lee, D.; Song, S.H.; Hwang, J.; Jin, S.H.; Park, K.H.; Kim, B.H.; Hong, S.H.; Jeon, S. Enhanced Mechanical Properties of Epoxy Nanocomposites by Mixing Non-covalently Functionalized Boron Nitride Nanoflakes. *Small* **2013**, *9*, 2602-2610, <https://doi.org/10.1002/sml.201203214>.
24. Mallakpour, S.; Zadehnazari, A. Functionalization of multi-wall carbon nanotubes with amino acid and its influence on the properties of thiadiazol bearing poly(amide-thioester-imide) composites. *Synthetic Metals* **2013**, *169*, 1-11, <https://doi.org/10.1016/j.synthmet.2013.03.002>.
25. Tian, W.; Liu, L.; Meng, F.; Liu, Y.; Li, Y.; Wang, F. The failure behaviour of an epoxy glass flake coating/steel system under marine alternating hydrostatic pressure. *Corrosion Science* **2014**, *86*, 81-92, <https://doi.org/10.1016/j.corsci.2014.04.038>.
26. Ladhari, A.; Ben Daly, H.; Belhadjsalah, H.; Cole, K.C.; Denault, J. Investigation of water absorption in clay-reinforced polypropylene nanocomposites. *Polymer Degradation and Stability* **2010**, *95*, 429-439, <https://doi.org/10.1016/j.polymdegradstab.2009.12.001>.
27. Bao, Y.; Ma, J.; Li, N. Synthesis and swelling behaviors of sodium carboxymethyl cellulose-g-poly(AA-co-AM-co-AMPS)/MMT superabsorbent hydrogel. *Carbohydrate Polymers* **2011**, *84*, 76-82, <https://doi.org/10.1016/j.carbpol.2010.10.061>.
28. Stephen, R.; Ranganathaiah, C.; Varghese, S.; Joseph, K.; Thomas, S. Gas transport through nano and micro composites of natural rubber (NR) and their blends with carboxylated styrene butadiene rubber (XSBR) latex membranes. *Polymer* **2006**, *47*, 858-870, <https://doi.org/10.1016/j.polymer.2005.12.020>.
29. Mohammed Altaweel, A.M.A.; Ranganathaiah, C.; Kothandaraman, B.; Raj, J.M.; Chandrashekhara, M.N. Characterization of ACS modified epoxy resin composites with fly ash and cenospheres as fillers: Mechanical and microstructural properties. *Polymer Composites* **2011**, *32*, 139-146, <https://doi.org/10.1002/pc.21030>.
30. Naebe, M.; Wang, J.; Amini, A.; Khayyam, H.; Hameed, N.; Li, L.H.; Chen, Y.; Fox, B. Mechanical Property and Structure of Covalent Functionalised Graphene/Epoxy Nanocomposites. *Scientific Reports* **2014**, *4*, <https://doi.org/10.1038/srep04375>.
31. Jiang, T.; Kuila, T.; Kim, N.H.; Ku, B.-C.; Lee, J.H. Enhanced mechanical properties of silanized silica nanoparticle attached graphene oxide/epoxy composites. *Composites Science and Technology* **2013**, *79*, 115-125, <https://doi.org/10.1016/j.compscitech.2013.02.018>.
32. Wu, C.L.; Zhang, M.Q.; Rong, M.Z.; Friedrich, K. Tensile performance improvement of low nanoparticles filled-polypropylene composites. *Composites Science and Technology* **2002**, *62*, 1327-1340, [https://doi.org/10.1016/S0266-3538\(02\)00079-9](https://doi.org/10.1016/S0266-3538(02)00079-9).
33. Chen, L.; Chai, S.; Liu, K.; Ning, N.; Gao, J.; Liu, Q.; Chen, F.; Fu, Q. Enhanced Epoxy/Silica Composites Mechanical Properties by Introducing Graphene Oxide to the Interface. *ACS Applied Materials & Interfaces* **2012**, *4*, 4398-4404, <https://doi.org/10.1021/am3010576>.
34. Dikobe, D.G.; Luyt, A.S. Effect of filler content and size on the properties of ethylene vinyl acetate copolymer-wood fiber composites. *Journal of Applied Polymer Science* **2007**, *103*, 3645-3654, <https://doi.org/10.1002/app.25513>.
35. Halpin, J.C. Stiffness and Expansion Estimates for Oriented Short Fiber Composites. *Journal of Composite Materials* **1969**, *3*, 732-734, <https://doi.org/10.1177/002199836900300419>.
36. Wang, F.; Drzal, L.T.; Qin, Y.; Huang, Z. Mechanical properties and thermal conductivity of graphene nanoplatelet/epoxy composites. *Journal of Materials Science* **2015**, *50*, 1082-1093, <https://doi.org/10.1007/s10853-014-8665-6>.
37. Al-Turaif, H.A. Effect of nano TiO₂ particle size on mechanical properties of cured epoxy resin. *Progress in Organic Coatings* **2010**, *69*, 241-246, <https://doi.org/10.1016/j.porgcoat.2010.05.011>.

38. Tang, L.-C.; Wan, Y.-J.; Yan, D.; Pei, Y.-B.; Zhao, L.; Li, Y.-B.; Wu, L.-B.; Jiang, J.-X.; Lai, G.-Q. The effect of graphene dispersion on the mechanical properties of graphene/epoxy composites. *Carbon* **2013**, *60*, 16-27, <https://doi.org/10.1016/j.carbon.2013.03.050>.
39. Gudarzi, M.M.; Sharif, F. Enhancement of dispersion and bonding of graphene-polymer through wet transfer of functionalized graphene oxide. *Express Polymer Letters*. **2012**, *6*.
40. Rostampour, A.; Sharif, M.; Mouji, N. Synergetic Effects of Graphene Oxide and Clay on the Microstructure and Properties of HIPS/Graphene Oxide/Clay Nanocomposites. *Polymer-Plastics Technology and Engineering* **2017**, *56*, 171-183, <https://doi.org/10.1080/03602559.2016.1185626>.
41. Javadi, S.; Sadroddini, M.; Razzaghi-Kashani, M.; Reis, P.N.B.; Balado, A.A. Interfacial effects on dielectric properties of ethylene propylene rubber–titania nano- and micro-composites. *Journal of Polymer Research* **2015**, *22*, <https://doi.org/10.1007/s10965-015-0805-4>.
42. Ramdani, N.; Derradji, M.; Wang, J.; Mokhnache, E.-O.; Liu, W.-B. Improvements of Thermal, Mechanical, and Water-Resistance Properties of Polybenzoxazine/Boron Carbide Nanocomposites. *JOM* **2016**, *68*, 2533-2542, <https://doi.org/10.1007/s11837-016-2040-9>.
43. Pourhossaini, M.-R.; Razzaghi-Kashani, M. Effect of silica particle size on chain dynamics and frictional properties of styrene butadiene rubber nano and micro composites. *Polymer* **2014**, *55*, 2279-2284, <https://doi.org/10.1016/j.polymer.2014.03.026>.
44. Zabihi, O.; Ahmadi, M.; Khayyam, H.; Naebe, M. Fish DNA-modified clays: Towards highly flame retardant polymer nanocomposite with improved interfacial and mechanical performance. *Scientific Reports* **2016**, *6*, <https://doi.org/10.1038/srep38194>.
45. Xu, B.; Fu, Y.Q.; Ahmad, M.; Luo, J.K.; Huang, W.M.; Kraft, A.; Reuben, R.; Pei, Y.T.; Chen, Z.G.; De Hosson, J.T.M. Thermo-mechanical properties of polystyrene-based shape memory nanocomposites. *Journal of Materials Chemistry* **2010**, *20*, 3442-3448, <https://doi.org/10.1039/B923238A>.
46. Zaman, I.; Phan, T.T.; Kuan, H.-C.; Meng, Q.; Bao La, L.T.; Luong, L.; Youssf, O.; Ma, J. Epoxy/graphene platelets nanocomposites with two levels of interface strength. *Polymer* **2011**, *52*, 1603-1611, <https://doi.org/10.1016/j.polymer.2011.02.003>.
47. Sadasivuni, K.K.; Ponnammam, D.; Kumar, B.; Strankowski, M.; Cardinaels, R.; Moldenaers, P.; Thomas, S.; Grohens, Y. Dielectric properties of modified graphene oxide filled polyurethane nanocomposites and its correlation with rheology. *Composites Science and Technology* **2014**, *104*, 18-25, <https://doi.org/10.1016/j.compscitech.2014.08.025>.
48. Pu, X.; Zhang, H.-B.; Li, X.; Gui, C.; Yu, Z.-Z. Thermally conductive and electrically insulating epoxy nanocomposites with silica-coated graphene. *RSC Advances* **2014**, *4*, 15297-15303, <https://doi.org/10.1039/C4RA00518J>.
49. Owen, M. Coupling agents: Chemical bonding at interfaces. *Adhesion Science and Engineering* **2002**, *2*, 403-431, <https://doi.org/10.1016/B978-044451140-9/50009-3>.
50. Wang, X.; Xing, W.; Zhang, P.; Song, L.; Yang, H.; Hu, Y. Covalent functionalization of graphene with organosilane and its use as a reinforcement in epoxy composites. *Composites Science and Technology* **2012**, *72*, 737-743, <https://doi.org/10.1016/j.compscitech.2012.01.027>.
51. Cao, Y.; Lai, Z.; Feng, J.; Wu, P. Graphene oxide sheets covalently functionalized with block copolymers via click chemistry as reinforcing fillers. *Journal of Materials Chemistry* **2011**, *21*, 9271-9278, <https://doi.org/10.1039/C1JM10420A>.
52. Monajjemi, M. Najafpour, J. Mollaamin, F. (3,3)4 Armchair carbon nanotube in connection with PNP and NPN junctions: Ab Initio and DFT-based studies, Fullerenes Nanotubes and Carbon Nanostructures, 2013, 21(3), 213-232 , DOI: 10.1080/1536383x.2011.597010
53. Mollaamin, F.; Monajjemi, M. DFT outlook of solvent effect on function of nano bioorganic drugs. *Physics and Chemistry of Liquids* **2012**, *50*, 596-604, <https://doi.org/10.1080/00319104.2011.646444>.
54. Mollaamin, F.; Gharibe, S.; Monajjemi, M. Synthesis of various nano and micro ZnSe morphologies by using hydrothermal method. *International Journal of Physical Sciences* **2011**, *6*, 1496-1500.
55. Monajjemi M. Graphene/(h-BN)*n*/X-doped raphene as anode material in lithium ion batteries (X = Li, Be, B AND N). *Macedonian Journal of Chemistry and Chemical Engineering* **2017**, *36*, 101–118, <http://dx.doi.org/10.20450/mjce.2017.1134>.
56. Monajjemi, M. Cell membrane causes the lipid bilayers to behave as variable capacitors: A resonance with self-induction of helical proteins. *Biophysical Chemistry* **2015**, *207*, 114-127, <https://doi.org/10.1016/j.bpc.2015.10.003>.
57. Monajjemi, M. Study of CD5+ Ions and Deuterated Variants (CH_xD(5-x)⁺): An Artefactual Rotation. *Russian Journal of Physical Chemistry A*, **2018**, *92*, 2215-2226.
58. Monajjemi, M. Liquid-phase exfoliation (LPE) of graphite towards graphene: An ab initio study. *Journal of Molecular Liquids* **2017**, *230*, 461–472, <https://doi.org/10.1016/j.molliq.2017.01.044>.
59. Jalilian, H.; Monajjemi, M. Capacitor simulation including of X-doped graphene (X = Li, Be, B) as two electrodes and (h-BN)*m* (*m* = 1–4) as the insulator. *Japanese Journal of Applied Physics* **2015**, *54*, 085101-7.

60. Ardalan, T.; Ardalan, P.; Monajjemi, M. Nano theoretical study of a C 16 cluster as a novel material for vitamin C carrier. *Fullerenes Nanotubes and Carbon Nanostructures* **2014**, *22*, 687-708, <https://doi.org/10.1080/1536383X.2012.717561>.
61. Mahdavian, L.; Monajjemi, M.; Mangkorntong, N. Sensor response to alcohol and chemical mechanism of carbon nanotube gas sensors *Fullerenes Nanotubes and Carbon Nanostructures* **2009**, *17*, 484-495, <https://doi.org/10.1080/15363830903130044>.
62. Monajjemi, M.; Najafpour, J. Charge density discrepancy between NBO and QTAIM in single-wall armchair carbon nanotubes. *Fullerenes Nanotubes and Carbon Nano structures* **2014**, *22*, 575-594, <https://doi.org/10.1080/1536383X.2012.702161>.
63. Monajjemi, M.; Hosseini, M.S. Non bonded interaction of B16 N16 nano ring with copper cations in point of crystal fields. *Journal of Computational and Theoretical Nanoscience* **2013**, *10*, 2473-2477.
64. Monajjemi, M.; Mahdavian, L.; Mollaamin, F. Characterization of nanocrystalline silicon germanium film and nanotube in adsorption gas by Monte Carlo and Langevin dynamic simulation. *Bulletin of the Chemical Society of Ethiopia* **2008**, *22*, 277-286, <https://doi.org/10.4314/bcse.v22i2.61299>.
65. Lee, V.S.; Nimmanpipug, P.; Mollaamin, F.; Thanasanvorakun, S.; Monajjemi, M. Investigation of single wall carbon nanotubes electrical properties and normal mode analysis: Dielectric effects. *Russian Journal of Physical Chemistry A* **2009**, *83*, 2288-2296, <https://doi.org/10.1134/S0036024409130184>.
66. Mollaamin, F.; Najafpour, J.; Ghadami, S.; Akrami, M.S.; Monajjemi, M. The electromagnetic feature of B N H (x = 0, 4, 8, 12, 16, and 20) nano rings: Quantum theory of atoms in molecules/NMR approach. *Journal of Computational and Theoretical Nanoscience* **2014**, *11*, 1290-1298.
67. Monajjemi, M.; Mahdavian, L.; Mollaamin, F.; Honarparvar, B. Thermodynamic investigation of enolketo tautomerism for alcohol sensors based on carbon nanotubes as chemical sensors. *Fullerenes Nanotubes and Carbon Nanostructures* **2010**, *18*, 45-55, <https://doi.org/10.1080/15363830903291564>.
68. Monajjemi, M.; Ghiasi, R.; Seyed, S.M.A. Metal-stabilized rare tautomers: N4 metalated cytosine (M = Li , Na , K , Rb and Cs), theoretical views. *Applied Organometallic Chemistry* **2003**, *17*, 635-640, <https://doi.org/10.1002/aoc.469>.
69. Ilkhani, A.R.; Monajjemi, M. The pseudo Jahn-Teller effect of puckering in pentatomic unsaturated rings C AE , A=N, P, As, E=H, F, Cl. *Computational and Theoretical Chemistry* **2015**, *1074*, 19-25, <http://dx.doi.org/10.1016%2Fj.comptc.2015.10.006>.
70. Monajjemi, M. Non-covalent attraction of B N and repulsion of B N in the B N ring: a quantum rotatory due to an external field. *Theoretical Chemistry Accounts* **2015**, *134*, 1-22, <https://doi.org/10.1007/s00214-015-1668-9>.
71. Monajjemi, M.; Naderi, F.; Mollaamin, F.; Khaleghian, M. Drug design outlook by calculation of second virial coefficient as a nano study. *Journal of the Mexican Chemical Society* **2012**, *56*, 207-211, <https://doi.org/10.29356/jmcs.v56i2.323>.
72. Monajjemi, M.; Bagheri, S.; Moosavi, M.S. Symmetry breaking of B2N(-,0,+): An aspect of the electric potential and atomic charges. *Molecules* **2015**, *20*, 21636-21657, <https://doi.org/10.3390/molecules201219769>.
73. Monajjemi, M.; Mohammadian, N.T. S-NICS: An aromaticity criterion for nano molecules. *Journal of Computational and Theoretical Nanoscience* **2015**, *12*, 4895-4914, <https://doi.org/10.1166/jctn.2015.4458>.
74. Monajjemi, M.; Ketabi, S.; Hashemian, Z.M.; Amiri, A. Simulation of DNA bases in water: Comparison of the Monte Carlo algorithm with molecular mechanics force fields. *Biochemistry (Moscow)* **2006**, *71*, 1-8, <https://doi.org/10.1134/s0006297906130013>.
75. Monajjemi, M.; Lee, V.S.; Khaleghian, M.; Honarparvar, B.; Mollaamin, F. Theoretical Description of Electromagnetic Nonbonded Interactions of Radical, Cationic, and Anionic NH2BHNBNH2 Inside of the B18N18 Nanoring. *J. Phys. Chem C* **2010**, *114*, 15315, <https://doi.org/10.1021/jp104274z>.
76. Monajjemi, M.; Boggs, J.E. A New Generation of BnNn Rings as a Supplement to Boron Nitride Tubes and Cages. *J. Phys. Chem. A* **2013**, *117*, 1670-1684, <http://dx.doi.org/10.1021/jp312073q>.
77. Monajjemi, M. Non bonded interaction between BnNn (stator) and BN B (rotor) systems: A quantum rotation in IR region. *Chemical Physics* **2013**, *425*, 29-45, <https://doi.org/10.1016/j.chemphys.2013.07.014>.
78. Monajjemi, M.; Robert, W.J.; Boggs, J.E. NMR contour maps as a new parameter of carboxyl's OH groups in amino acids recognition: A reason of tRNA-amino acid conjugation. *Chemical Physics* **2014**, *433*, 1-11, <https://doi.org/10.1016/j.chemphys.2014.01.017>.
79. Monajjemi, M. Quantum investigation of non-bonded interaction between the B15N15 ring and BH2NBH2 (radical, cation, and anion) systems: a nano molecular motor. *Struct Chem* **2012**, *23*, 551-580, <http://dx.doi.org/10.1007/s11224-011-9895-8>.
80. Monajjemi, M. Metal-doped graphene layers composed with boron nitride-graphene as an insulator: a nano-capacitor. *Journal of Molecular Modeling* **2014**, *20*, <https://doi.org/10.1007/s00894-014-2507-y>.
81. Mollaamin, F.; Monajjemi, M.; Mehrzad, J. Molecular Modeling Investigation of an Anti-cancer Agent Joint to SWCNT Using Theoretical Methods. *Fullerenes nanotubes and carbon nanostructures* **2014**, *22*, 738-751, <https://doi.org/10.1080/1536383X.2012.731582>.

82. Monajjemi, M.; Ketabi, S.; Amiri, A. Monte Carlo simulation study of melittin: protein folding and temperature dependence, *Russian journal of physical chemistry* **2006**, *80*, S55-S62, <https://doi.org/10.1134/S0036024406130103>.
83. Monajjemi, M.; Heshmata, M.; Haeria, H.H. QM/MM model study on properties and structure of some antibiotics in gas phase: Comparison of energy and NMR chemical shift. *Biochemistry-moscow* **2006**, *71*, S113-S122, <https://doi.org/10.1134/S0006297906130190>.
84. Monajjemi, M.; Afsharnezhad, S.; Jaafari, M.R.; Abdolahi, A.N.; Monajemi, H. NMR shielding and a thermodynamic study of the effect of environmental exposure to petrochemical solvent on DPPC, an important component of lung surfactant. *Russian journal of physical chemistry A* **2007**, *81*, 1956-1963, <https://doi.org/10.1134/S0036024407120096>.
85. Mollaamin, F.; Noei, M.; Monajjemi, M.; Rasoolzadeh, R. Nano theoretical studies of fMet-tRNA structure in protein synthesis of prokaryotes and its comparison with the structure of fAla-tRNA. *African journal of microbiology research* **2011**, *5*, 2667-2674, <https://doi.org/10.5897/AJMR11.310>.
86. Monajjemi, M.; Heshmat, M.; Haeri, H.H.; Kaveh, F. Theoretical study of vitamin properties from combined QM-MM methods: Comparison of chemical shifts and energy. *Russian Journal of Physical Chemistry* **2006**, *80*, 1061-1068, <https://doi.org/10.1134/S0036024406070119>.
87. Monajjemi, M.; Chahkandi, B. Theoretical investigation of hydrogen bonding in Watson-Crick, Hoogsteen and their reversed and other models: comparison and analysis for configurations of adenine-thymine base pairs in 9 models. *Journal of molecular structure-theochem* **2005**, *714*, 43-60, <https://doi.org/10.1016/j.theochem.2004.09.048>.
88. Monajjemi, M.; Honarparvar, B.; Haeri, H.H.; Heshmat, M. An ab initio quantum chemical investigation of solvent-induced effect on N-14-NQR parameters of alanine, glycine, valine, and serine using a polarizable continuum model. *Russian journal of physical chemistry* **2006**, *80*, S40-S44, <https://doi.org/10.1134/S0036024406130073>.
89. Monajjemi, M.; Seyed Hosseini, M. Non Bonded Interaction of B₁₆N₁₆ Nano Ring with Copper Cations in Point of Crystal Fields. *Journal of Computational and Theoretical Nanoscience* **2013**, *10*, 2473-2477, <https://doi.org/10.1166/jctn.2013.3233>.
90. Monajjemi, M.; Farahani, N.; Mollaamin, F. Thermodynamic study of solvent effects on nanostructures: phosphatidylserine and phosphatidylinositol membranes. *Physics and chemistry of liquids* **2012**, *50*, 161-172, <https://doi.org/10.1080/00319104.2010.527842>.
91. Monajjemi, M.; Ahmadianarog, M. Carbon Nanotube as a Deliver for Sulforaphane in Broccoli Vegetable in Point of Nuclear Magnetic Resonance and Natural Bond Orbital Specifications. *Journal of computational and theoretical nanoscience* **2014**, *11*, 1465-1471, <https://doi.org/10.1166/jctn.2014.3519>.
92. Monajjemi, M.; Ghiasi, R.; Ketabi, S.; Passdar, H.; Mollaamin, F. A Theoretical Study of Metal-Stabilised Rare Tautomers Stability: N4 Metalated Cytosine (M=Be²⁺, Mg²⁺, Ca²⁺, Sr²⁺ and Ba²⁺) in Gas Phase and Different Solvents. *Journal of Chemical Research* **2004**, *1*, 11-18, <https://doi.org/10.3184/030823404323000648>.
93. Monajjemi, M.; Baei, M.T.; Mollaamin, F. Quantum mechanic study of hydrogen chemisorptions on nanocluster vanadium surface. *Russian journal of inorganic chemistry* **2008**, *53*, 1430-1437, <https://doi.org/10.1134/S0036023608090143>.
94. Mollaamin, F.; Baei, M.T.; Monajjemi, M.; Zhiani, R.; Honarparvar, B. A DFT study of hydrogen chemisorption on V (100) surfaces. *Russian Journal Of Physical Chemistry A* **2008**, *82*, 2354-2361, <https://doi.org/10.1134/S0036024408130323>.
95. Monajjemi, M.; Honarparvar, B.; Nasser, S.M.; Khaleghian, M. NQR and NMR study of hydrogen bonding interactions in anhydrous and monohydrated guanine cluster model: A computational study. *Journal of structural chemistry* **2009**, *50*, 67-77, <https://doi.org/10.1007/s10947-009-0009-z>.
96. Monajjemi, M.; Aghaie, H.; Naderi, F. Thermodynamic study of interaction of TSPP, CoTsPc, and FeTsPc with calf thymus DNA. *Biochemistry-Moscow* **2007**, *72*, 652-657, <https://doi.org/10.1134/S0006297907060089>.
97. Monajjemi, M.; Heshmat, M.; Aghaei, H.; Ahmadi, R.; Zare, K. Solvent effect on N-14 NMR shielding of glycine, serine, leucine, and threonine: Comparison between chemical shifts and energy versus dielectric constant. *Bulletin of the chemical society of ethiopia* **2007**, *21*, 111-116, <https://doi.org/10.4314/bcse.v21i1.61387>.
98. Monajjemi, M.; Rajaeian, E.; Mollaamin, F.; Naderi, F.; Saki, S. Investigation of NMR shielding tensors in 1,3 dipolar cycloadditions: solvents dielectric effect. *Physics and chemistry of liquids* **2008**, *46*, 299-306, <https://doi.org/10.1080/00319100601124369>.
99. Mollaamin, F.; Varmaghani, Z.; Monajjemi, M. Dielectric effect on thermodynamic properties in vinblastine by DFT/Onsager modelling. *Physics and chemistry of liquids* **2011**, *49*, 318-336, <https://doi.org/10.1080/00319100903456121>.
100. Monajjemi, M.; Honarparvar, B.; Hadad, B.K.; Ilkhani, A.R.; Mollaamin, F. Thermo-chemical investigation and NBO analysis of some anxiolytic as Nano-drugs. *African journal of pharmacy and pharmacology* **2010**, *4*, 521-529.

101. Monajjemi, M.; Khaleghian, M.; Mollaamin, F. Theoretical study of the intermolecular potential energy and second virial coefficient in the mixtures of CH₄ and Kr gases: a comparison with experimental data. *Molecular simulation* **2010**, *11*, 865-870, <https://doi.org/10.1080/08927022.2010.489557>.
102. Monajjemi, M.; Khosravi, M.; Honarparvar, B.; Mollamin, F. Substituent and Solvent Effects on the Structural Bioactivity and Anticancer Characteristic of Catechin as a Bioactive Constituent of Green Tea. *International journal of quantum chemistry* **2011**, *111*, 2771-2777.
103. Tahan, A.; Monajjemi, M. Solvent Dielectric Effect and Side Chain Mutation on the Structural Stability of Burkholderia cepacia Lipase Active Site: A Quantum Mechanical/ Molecular Mechanics Study. *Biotheoretica* **2011**, *59*, 291-312, <https://doi.org/10.1007/s10441-011-9137-x>.
104. Monajjemi, M.; Khaleghian, M. EPR Study of Electronic Structure of [CoF₆](3-) and B18N18 Nano Ring Field Effects on Octahedral Complex. *Journal of cluster science* **2011**, *22*, 673-692, <https://doi.org/10.1007/s10876-011-0414-2>.
105. Monajjemi, M.; Mollaamin, F. Molecular Modeling Study of Drug-DNA Combined to Single Walled Carbon Nanotube, *Journal of cluster science* **2012**, *23*, 259-272, <https://doi.org/10.1007/s10876-011-0426-y>.
106. Mollaamin, F.; Monajjemi, M. Fractal Dimension on Carbon Nanotube-Polymer Composite Materials Using Percolation Theory. *Journal of computational and theoretical nanoscience* **2012**, *9*, 597-601, <https://doi.org/10.1166/jctn.2012.2067>.
107. Mahdavian, L.; Monajjemi, M. Alcohol sensors based on SWNT as chemical sensors: Monte Carlo and Langevin dynamics simulation. *Microelectronics journal* **2010**, *41*, 142-149, <https://doi.org/10.1016/j.mejo.2010.01.011>.
108. Monajjemi, M.; Falahati, M.; Mollaamin, F. Computational investigation on alcohol nanosensors in combination with carbon nanotube: a Monte Carlo and ab initio simulation. *Ionics* **2013**, *19*, 155-164, <https://doi.org/10.1007/s11581-012-0708-x>.
109. Lee, C.; Wei, X.; Kysar, J. W.; Hone, J. Measurement of the Elastic Properties and Intrinsic Strength of Monolayer Graphene. *Science* **2008**, *321*, <https://doi.org/10.1126/science.1157996>.
110. Gou, J.; Minaie, B.; Wang, B.; Liang, Z.; Zhang, Computational and experimental study of interfacial bonding of single-walled nanotube reinforced composites C. *Comput. Mater. Sci.* **2004**, *31*, 3, 4, 225-236, <https://doi.org/10.1016/j.compmatsci.2004.03.002>.
111. Sampath, P.; Santhanam, S.K.V. Effect of moringa and bagasse ash filler particles on basalt/epoxy composites. *Pol ímeros* **2019**, *29*, <https://doi.org/10.1590/0104-1428.01219>.
112. Bulut, M.; Bozkurt, Ö.Y.; Erklı̇g, A.; Yayka, S.H.; Özbek, Ö. Mechanical and Dynamic Properties of Basalt Fiber-Reinforced Composites with Nanoclay Particles. *Arab. J. Sci. Eng.* **2020**, *45*, 1017-1033, <https://doi.org/10.1007/s13369-019-04226-6>.
113. Ulus, H.; Kaybal, H.B.; Eskizeybek, V.; Avcı, A. Enhanced Salty Water Durability of Halloysite Nanotube Reinforced Epoxy/Basalt Fiber Hybrid Composites. *Fibers Polym.* **2019**, *20*, 2184-2199, <https://doi.org/10.1007/s12221-019-9316-y>.
114. Toorchi, D.; Khosravi, H.; Tohidlou, E. Synergistic effect of nano-ZrO₂/graphene oxide hybrid system on the high-velocity impact behavior and interlaminar shear strength of basalt fiber/epoxy composite. *J. Ind. Text.* **2019**, <https://doi.org/10.1177/1528083719879922>.
115. Kumar, C.V.; Kandasubramanian, B. Advances in Ablative Composites of Carbon Based Materials: A Review. *Ind. Eng. Chem. Res.* **2019**, *58*, 22663-22701, <https://doi.org/10.1021/acs.iecr.9b04625>.
116. Naidu, P.P.; Raghavendra, G.; Ojha, S.; Paplal, B. Effect of g-C 3 N 4 nanofiller as filler on mechanical properties of multidirectional glass fiber epoxy hybrid composites. *J. Appl. Polym. Sci.* **2020**, *137*, <https://doi.org/10.1002/app.48413>.
117. Parveen, S.; Pichandi, S.; Goswami, P.; Rana, S. Novel glass fibre reinforced hierarchical composites with improved interfacial, mechanical and dynamic mechanical properties developed using cellulose microcrystals. *Mater. Des.* **2020**, *188*, <https://doi.org/10.1016/j.matdes.2019.108448>.
118. Bagci, M.; Demirci, M.; Sukur, E.F.; Kaybal, H.B. The effect of nanoclay particles on the incubation period in solid particle erosion of glass fibre/epoxy nanocomposites. *Wear* **2020**, *444*, <https://doi.org/10.1016/j.wear.2019.203159>.
119. Domun, N.; Kaboglu, C.; Paton, K.R.; Dear, J.P.; Liu, J.; Blackman, B.R.K.; Liaghat, G.; Hadavinia, H. Ballistic impact behaviour of glass fibre reinforced polymer composite with 1D/2D nanomodified epoxy matrices. *Compos. Part B Eng.* **2019**, *167*, 497-506, <https://doi.org/10.1016/j.compositesb.2019.03.024>.
120. Burda, I.; Barbezat, M.; Brunner, A.J. Delamination resistance of GFRP-epoxy rods with nanoparticle- and microparticle-modified matrix and its correlation with the fracture properties of epoxy nanocomposites. *Fatigue Fract. Eng. Mater. Struct.* **2020**, *43*, 292-307, <https://doi.org/10.1111/ffe.13122>.
121. Chaudhary, V.; Bajpai, P.K.; Maheshwari, S. Effect of moisture absorption on the mechanical performance of natural fiber reinforced woven hybrid bio-composites. *J. Nat. Fibers* **2020**, *17*, 84-100, <https://doi.org/10.1080/15440478.2018.1469451>.
122. Barczewski, M.; Sałasińska, K.; Szulc, J. Application of sunflower husk, hazelnut shell and walnut shell as waste agricultural fillers for epoxy-based composites: A study into mechanical behavior related to structural and rheological properties. *Polym. Test.* **2019**, *75*, 1-11, <https://doi.org/10.1016/j.polymertesting.2019.01.017>.

123. Khotbehsara, M.M.; Manalo, A.; Aravinthan, T.; Reddy, K.R.; Ferdous, W.; Wong, H.; Nazari, A. Effect of elevated in-service temperature on the mechanical properties and microstructure of particulate-filled epoxy polymers. *Polym. Degrad. Stab.* **2019**, *170*, <https://doi.org/10.1016/j.polymdegradstab.2019.108994>.
124. Katafiasz, T.J.; Iannucci, L.; Greenhalgh, E.S. Development of a novel compact tension specimen to mitigate premature compression and buckling failure modes within fibre hybrid epoxy composites. *Compos. Struct.* **2019**, *207*, 93–107, <https://doi.org/10.1016/j.compstruct.2018.06.124>.
125. Doddi, P.R.V.; Chanamala, R.; Dora, S.P. Effect of fiber orientation on dynamic mechanical properties of PALF hybridized with basalt reinforced epoxy composites. *Mater. Res. Express* **2020**, *7*, <https://doi.org/10.1088/2053-1591/ab6771>.